crystals

MDPI

Review

Voltage Control of Exchange Bias via Magneto-Ionic Approaches

Yifu Luo [1,2], Shengsheng Liu [1], Yuxin Li [1], Zhen Wang [1], Jie Zhang [1,*] and Limei Zheng [2,*]

[1] Department of Physics and Electronic Engineering, Chongqing Normal University, Chongqing 401331, China; yifuluo821@gmail.com (Y.L.); lss2263163783@163.com (S.L.); t15158006133@163.com (Y.L.); zhenwang19990121@163.com (Z.W.)
[2] Department of Physics, Shandong University, Jinan 250100, China
* Correspondence: jiezhang@cqnu.edu.cn (J.Z.); zhenglm@sdu.edu.cn (L.Z.)

Abstract: The exchange bias (EB) effect denotes a magnetic bias phenomenon originating from the interfacial exchange coupling at the ferromagnetic/antiferromagnetic materials, which plays an indispensable role in the functionality of various devices, such as magnetic random-access memory (MRAM) and sensors. Voltage control of exchange bias offers a promising pathway to significantly reduce device power consumption, effectively fostering the evolution of low-energy spintronic devices. The "magneto-ionic" mechanism, characterized by its operational efficiency, low energy consumption, reversibility, and non-volatility, provides innovative approaches for voltage control of exchange bias and has led to a series of significant advancements. This review systematically synthesizes the research progress on voltage control of exchange bias based on the magneto-ionic mechanism from the perspectives of ionic species, material systems, underlying mechanisms, and performance parameters. Furthermore, it undertakes a comparative evaluation of the voltage-controlled exchange bias by different ions, ultimately providing a forward-looking perspective on the future trajectory of this research domain.

Keywords: spintronics; voltage control of magnetism; magneto-ionic mechanism; exchange bias

Academic Editor: Yulia V. Nelyubina

Received: 21 December 2024
Revised: 8 January 2025
Accepted: 11 January 2025
Published: 14 January 2025

Citation: Luo, Y.; Liu, S.; Li, Y.; Wang, Z.; Zhang, J.; Zheng, L. Voltage Control of Exchange Bias via Magneto-Ionic Approaches. *Crystals* **2025**, *15*, 77. https://doi.org/10.3390/cryst15010077

1. Introduction

With the continuous proliferation of modern electronic devices and the relentless emergence of various intelligent communication technologies, the development of data storage and retrieval devices has become a crucial driver of progress in the field of information materials. Spintronics, which utilizes both electron charge and spin as carriers of information, is considered an effective strategy for the creation of next-generation electronic devices [1,2]. The electric field can directly interact with charges, affecting the spin, thereby facilitating the effective modulation of magnetism and electrical transport of magnetic materials, which plays a vital role in information storage technology. Over the years, the number of materials and mechanisms related to electric field-controlled magnetism has steadily increased, gradually evolving into a research domain that is broadly classified as voltage control of magnetism (VCM) [3].

Exchange bias (EB) is a spin-pinning phenomenon observed at ferromagnetic (FM)/antiferromagnetic (AFM) interfaces [4], while the spin exchange coupling between adjacent layers induces a shift in the hysteresis loop relative to the zero field, accompanied by an increase in coercivity [5]. FM/AFM multilayer heterostructures exhibiting exchange bias effects have been widely applied in modern spintronic devices, such as hard disk read heads, magnetic random-access memory, and tunnel magnetoresistance sensors, forming a

crucial foundation in the field of information storage [6,7]. Utilizing electric fields in place of magnetic fields or currents to modulate exchange bias can substantially reduce device power consumption. This approach can significantly propel the development of high-speed, low-energy, and non-volatile spintronic devices, thereby attracting considerable attention from researchers worldwide [8].

The inverse magnetoelectric coupling effect in single-phase multiferroic materials and ferroelectric (FE)/ferromagnetic (FM) composite multiferroic heterostructures are two pivotal methods for achieving electric field control of exchange bias, as depicted in Figure 1 [8–10]. Single-phase multiferroic materials (e.g., Cr_2O_3 [11–13], $YMnO_3$ [14], $BiFeO_3$ [15–17]) exhibit both ferroelectric/dielectric and antiferromagnetic properties below the Néel temperature. In terms of single-phase multiferroic/ferromagnetic heterojunctions, electric field control of the polarization state induces changes in antiferromagnetic domains through the intrinsic coupling of ferroelectricity and antiferromagnetism, thereby enabling effective modulation of exchange bias (Figure 1a) [11–16]. However, single-phase multiferroic materials with strong magnetoelectric coupling effects at room temperature (RT) have yet to be discovered, suggesting that practical device applications are still far off. As for FE/FM multiferroic heterojunctions, the lattice changes in ferroelectric materials (e.g., $BaTiO_3$ [18], $Pb(Mg_{1/3}Nb_{2/3})_{0.7}Ti_{0.3}O_3$ [19]) induced by the electric field-generated stress could be transferred to the ferromagnetic layer by magnetostrictive effects, altering its magnetism and consequently modifying the exchange bias in FE/FM/AFM multilayer heterojunctions (Figure 1b) [18,19]. However, the stress mechanism-based modulation of exchange bias in FE/FM multiferroic heterojunctions requires voltages in the orders of kV ~MV, which can readily lead to device fatigue or breakdown. Moreover, the stringent requirements for thin film growth conditions further constrain its practical applications. Additionally, in the [Co/Pt]/IrMn and [Co/Pt]/FeMn systems, Song et al. [20,21] utilized ionic liquids (IL) as gate electrodes to modify the surface carrier concentration of the antiferromagnetic layer. This modification controls the exchange bias through the formation of exchange springs within the antiferromagnetic layer. Nevertheless, the modulation based on this electrostatic doping method is volatile. Subsequently, Liu et al. [22] explored the generation and migration of oxygen vacancies induced by IL gating within the designed Pt/IrMn/Co/Pt/Ta antiferromagnetic thin films to enhance the voltage control effect of perpendicular exchange bias. At RT, they observed a reversible and non-volatile exchange bias field (H_{EB} = 560 Oe) and attributed it to the combined effects of electrostatic doping and ion migration. This result provides a novel approach to electric field control of exchange bias.

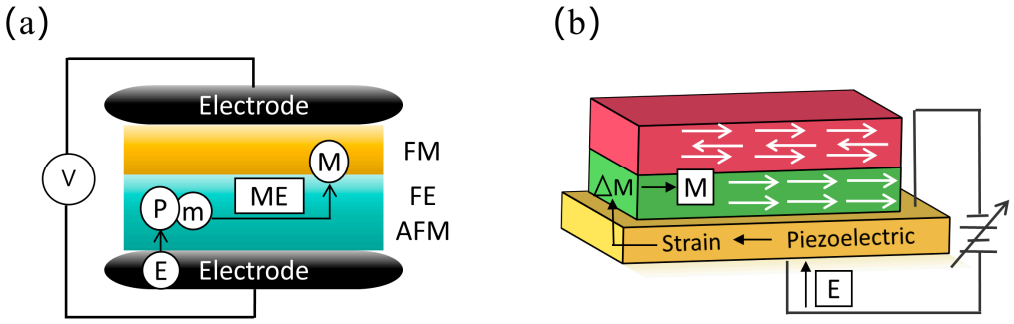

Figure 1. Schematic of two pivotal approaches (The arrows in the schematic illustrate the steps in−volved in electric field modulation of exchange bias). (**a**) Electric field control of exchange bias by single-phase magnetoelectric materials; (**b**) Electric field control of exchange bias based on FE/FM composite multiferroic heterostructures.

In recent years, the evolution of spintronics has continually stimulated the emergence of new VCM mechanisms, providing novel methods for voltage control of exchange bias. In 2014, Bauer et al. [23] utilized GdO_x as gating material for VCM, which has high oxygen mobility as a solid electrolyte of fuel cells [24]. By voltage-driven migration of oxygen ions, they altered the oxidation state at the GdO_x/Co interface, achieving electric field control of the saturation magnetization (M_S) and perpendicular magnetic anisotropy (PMA) of the ultrathin Co layer. Consequently, a novel electric control magnetic mechanism termed the "magneto-ionic" mechanism was proposed [23,24]. Figure 2 schematically illustrates the magneto-ionic mechanism, which employs liquid/solid electrolytes with high ion mobilities, such as IL, GdO_x [23–25], yttria-stabilized zirconia [26], $SrCoO_{2.5}$ [27], and $LiPF_6$ [28]. The ions in the electrolytes or target materials (e.g., O^{2-} [29–31], Li^+ [32–34], H^+ [35,36], F^- [37], N^{3-} [38]) are driven to migrate into/out of the target material by applied voltage, resulting in changes of crystal lattice, elemental valence states, spin arrangements, etc., which can lead to the evolution of the target materials' magnetic properties, including coercivity, M_S, magnetic anisotropy (MA), the Dzyaloshinsky–Moriya interaction (DMI), exchange bias, domain wall motion velocity, and so on [23–28,39,40]. In comparison to other VCM mechanisms, the magneto-ionic mechanism not only offers the advantages of low applied voltage and non-volatility but also exhibits substantial improvements in the depth of effect and amplitude of modulation [29–38]. Although there already have been some reviews on electric field control of magnetism that involved magneto-ionic approaches [41–44], a comprehensive introduction of voltage control of exchange bias via magneto-ionic approaches is lacking. This review will commence with a concise introduction to the origins, phenomena, and theoretical models of the exchange bias effect. In the following section, the vital and latest advancements in the field of voltage-controlled exchange bias will be discussed from the perspective of ion species associated with magneto-ionic mechanism. Finally, we will conclude with a prospective outlook on the development trends within this field.

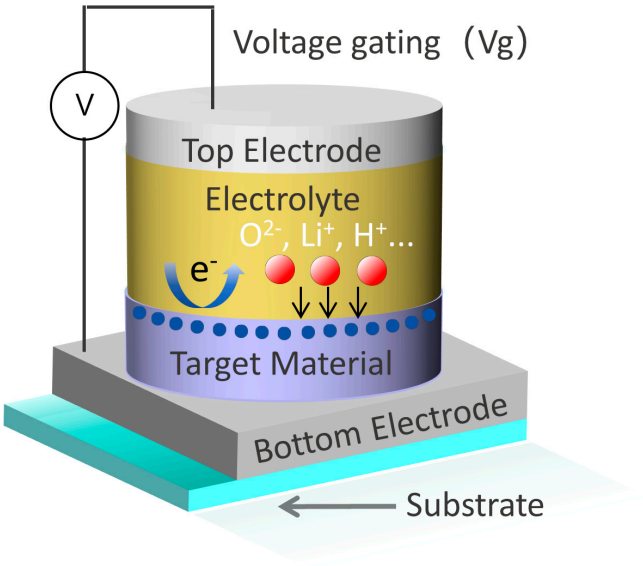

Figure 2. Schematic of magneto-ionic mechanism. By using liquid/solid electrolytes with high ion mobility, the gate voltage (Vg) can control the magnetic properties of the target materials via ions transport (red circles represent ions like O^{2-}, Li^+, H^+, and so on).

2. Exchange Bias Effect

In 1956, Meiklejohn and Bean [45] discovered the exchange bias effect while studying Co/CoO core-shell nanostructures, initiating over half a century of research into this phe-

nomenon. By the late 20th century, the exchange bias effect had been widely applied in spin valve structures based on the giant magnetoresistance (GMR) effect [46], marking a crucial step from material science to device applications. Today, it has become a fundamental component in the field of information storage and finds extensive applications across various fields [5–7].

As shown in Figure 3, the exchange bias effect is typically believed to originate from the direct exchange coupling at the FM/AFM interface, where the uncompensated magnetic moments of the AFM layer exert a pinning effect on the magnetic moments of the FM layer, thereby hindering their reversal (the schematic illustrates only the process of positive exchange bias, whereas negative exchange bias is characterized by both the magnetization and pinning directions being reversed). As shown in Figure 4, To elucidate the microscopic physical mechanisms underlying the exchange bias effect, Meiklejohn and Bean [47] proposed the inaugural theoretical model, known as the M-B model. This model hypothesizes that the spins in the FM layer rotate uniformly under a magnetic field, and that both the spin orientation in the ferromagnetic layer, as well as the spin direction of the antiferromagnetic neutron lattice, is uniformly aligned throughout the entire sample. The free energy of the FM/AFM bilayer system is given by the following equation:

$$E = -HM_{FM}t_{FM}\cos(\theta - \beta) + K_{AFM}t_{AFM}sin^2\alpha - J_{ex}\cos(\beta - \alpha) \quad (1)$$

wherein H represents the external magnetic field, M_{FM} is the magnetization of the FM layer, and t_{FM} and t_{AFM} are the respective thicknesses of the FM and AFM layers. K_{AFM} denotes the uniaxial anisotropy constant of the AFM layer. The first two terms correspond to the Zeeman energy of the FM layer and the uniaxial anisotropy energy of the AFM layer, respectively, while the third term J_{ex}, signifies the interfacial exchange coupling energy between the FM and AFM layers. Calculations from the M-B model indicate that exchange bias field emerges when t_{AFM} surpasses a critical threshold, specifically $t_{AFM} \geq J_{ex}/K_{AFM}$, or when K_{AFM} approaches infinity. The expression for the exchange bias field is defined as

$$H_E = \frac{J_{ex}}{t_{FM} \cdot M_{FM}} \quad (2)$$

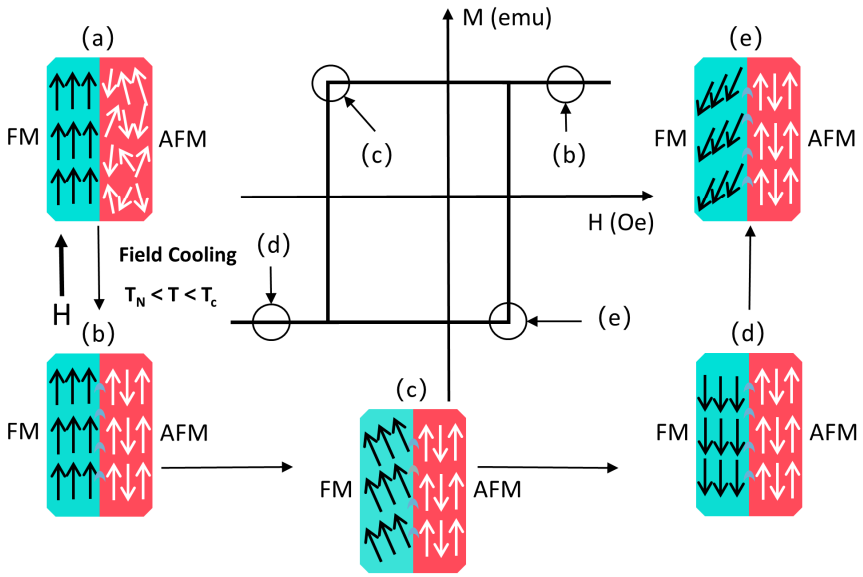

Figure 3. Schematic of microscopic mechanism of exchange bias effect. (**a**–**e**) represent the magnetic reversal process of an FM/AFM bilayer film system after field cooling with additional magnetic field assistance.

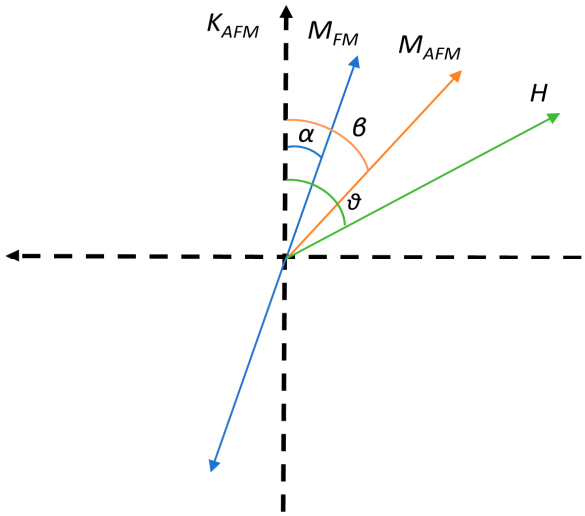

Figure 4. Schematic representation of the angular configuration in the exchange bias system of the M-B model, where the magnetization of the AFM layer exhibits two inverse orientations.

Whether in single-crystal or polycrystalline AFM thin film heterojunctions, experiments demonstrate that their surface net magnetic moment is merely one percent of that of an ideal uncompensated interface. Conversely, the exchange bias field calculated from Equation (2) surpasses the experimental results by 2–3 orders of magnitude and fails to reflect the influence of the AFM layer parameters.

To address the theoretical and experimental discrepancies, Mauri et al. [48] proposed the antiferromagnetic domain wall model in 1987. They posited the following assumptions: (a) the AFM layer thickness approaches infinity; (b) the spin reversal in the FM layer is perfectly coherent; and (c) an AFM domain wall parallel to the FM/AFM interface can form. Consequently, the free energy equation can be expressed as follows:

$$E = -\delta_w \cos\alpha - HM_{FM}t_{FM}\cos(\theta - \beta) + K_{AFM}t_{AFM}sin^2\alpha - J_{ex}\cos(\beta - \alpha) \quad (3)$$

where the four terms correspond to the AFM domain wall energy, the Zeeman energy of the FM layer, the uniaxial anisotropy energy of the AFM layer, and the interfacial coupling energy, respectively. As the spins in the FM layer rotate under the influence of a magnetic field, the spins within the AFM layer form a domain wall structure, resulting in increased system energy. Calculations indicate that the domain wall energy per unit area is $\delta_w = \sqrt{A_{AFM} \cdot K_{AFM}}$, where A_{AFM} denotes the exchange constant. In the case of strong coupling, where the interfacial coupling energy (J_{ex}) significantly exceeds the domain wall energy (δ_w), the expression for the exchange bias field is defined as

$$H_E = -2\left[\frac{\sqrt{A_{AFM} \cdot K_{AFM}}}{M_{FM} \cdot t_{FM}}\right] \quad (4)$$

Equation (4) effectively elucidates the intrinsic relationship between the parameters of the AFM layer and the exchange bias field. Furthermore, under strong coupling conditions, the model assumes the formation of a domain wall structure parallel to the interface within the AFM layer, reducing the calculated energy by approximately $\pi \cdot \frac{\sqrt{A_{AFM} \cdot K_{AFM}}}{\alpha} \approx 100$ times. As a result, the theoretical value of H_E closely approximates the experimental findings, overcoming the limitations of the M-B model. However, this model only considers the scenario of uncompensated interfaces, where the net magnetic moment at the AFM interface is non-zero, and fails to elucidate the occurrence of exchange bias at compensated interfaces where the net magnetic moment is zero. Subsequently, to

address this practical situation, and considering that real interfaces inevitably possess lattice defects or roughness, Malozemoff [49] proposed the random field model to qualitatively explain exchange bias in FM/AFM bilayers. The author contends that if the AFM is in single-domain state, the average effect of the exchange interaction field in an FM/AFM system with a compensated interface would be null over a macroscopic scale. However, it has been demonstrated that due to lattice defects or roughness at the AFM interface, the spin distribution at the atomic scale is non-uniform, resulting in a net magnetic moment even at a compensated interface. The uncompensated spins in the AFM layer are exchange coupled with the spins in the FM layer, causing the FM spins to exert a random field effect on the AFM layer. This model explains phenomena such as the linear decrease of the exchange bias field with temperature/blocking temperature (T/T_B) and the presence of a critical thickness for the AFM layer influencing the exchange bias field. Although the theoretical values provided by the new model are closer to experimental results, it remains insufficient to explain all exchange bias systems, necessitating the development of more comprehensive theoretical models to solve practical issues [4,50].

3. Voltage-Controlled Exchange Bias Based on Magneto-Ionic Mechanism

In this section, we shall explore the significant and most recent advancements in the field of voltage control of exchange bias, specifically from the perspective of ion species associated with magneto-ionic mechanism. These ions, including O^{2-}, H^+, Li^+, F^-, and N^{3-}, play a pivotal role in modulating the exchange bias. This discussion will integrate various dimensions, encompassing material systems, underlying mechanisms, and performance metrics.

3.1. Voltage-Controlled Exchange Bias Based on Oxygen Ions

3.1.1. Ionic Liquid Gating

The magneto-ionic mechanism based on O^{2-} plays a crucial role in VCM [29–31,41,42]. As previously mentioned, the magneto-ionic mechanism originates from the modulation of magnetism by electric field-driven O^{2-} migration. As reported, Gadolinium (Gd) possesses a high affinity for oxygen, readily combining with O^{2-} to form GdO_x, which is an excellent conductor for O^{2-} migration [51]. Liu et al. [52] utilized the oxygen affinity of Gd to induce the interfacial of adjacent layer transforming from oxidized $Ni_{1-x}Co_xO$ to ferromagnetic NiCo in Gd/$Ni_{1-x}Co_xO$ heterostructures. The electron energy loss spectroscopy (EELS) measurement confirmed the formation of a NiCo layer. The Gd/$Ni_{0.33}Co_{0.67}O$ bilayer film was heated to 400 K and subsequently cooled to RT under a 10 kOe magnetic field, resulting in an exchange bias field of −80 Oe and a coercivity of 276 Oe. The application of a gating voltage (Vg, 20 V) enhanced the modulation amplitude by 35%, exhibiting reversibility upon thermal cycling. Additionally, they further investigated the synergistic impact of Helium (He) ions irradiation and oxygen implantation on the exchange bias of Gd/$Ni_{0.33}Co_{0.67}O$ bilayer films [53]. The research demonstrates that He^+ irradiation induces lattice expansion in the NiCoO layer due to stress relaxation, thereby altering the diffusion rate of O^{2-} and the amplitude of the exchange bias field. On the other hand, the injection of O^{2-} leads to lattice contraction and phase separation within the NiCoO layer, forming NiO- and CoO-enriched regions, which enables the modulation of the exchange bias at RT. Although electrolyte materials such as GdO_x exhibit high O^{2-} mobility, the migration of O^{2-} still needs the assistance of high voltages or elevated temperatures, which hinders efforts to reduce device power consumption.

In 2013, Parkin et al. [54] observed that in IL gated epitaxial VO_2 thin films the large electric field generated by the ultrathin electric double layer (EDL) at the IL/VO_2 interface,

characterized by oppositely paired charges could drive the oxygen out of the film and led to the formation of oxygen vacancies. As shown in Figure 5, Cui et al. [55–57] demonstrated that in IL-gated $La_{0.5}Sr_{0.5}MnO_3$ (LSMO)/STO heterostructures, the application of a small voltage enables ex situ observation of changes in orbital occupancy under an electric field, thereby achieving non-volatile control of the MA and M_S of the LSMO. The modulation effect is manifested by the switching of the easy axis of LSMO from in-plane (IP) to out-of-plane (OOP) as the Vg varies from −3 V to +3 V, accompanied by the corresponding M_S increasing from 47.2 emu/cm^3 to 78.4 emu/cm^3 under negative voltage. The non-volatility of orbital occupancy manipulation under the IL gating verified the regulation mechanism of O^{2-}/oxygen vacancies (O_V) migration rather than simple electrostatic doping.

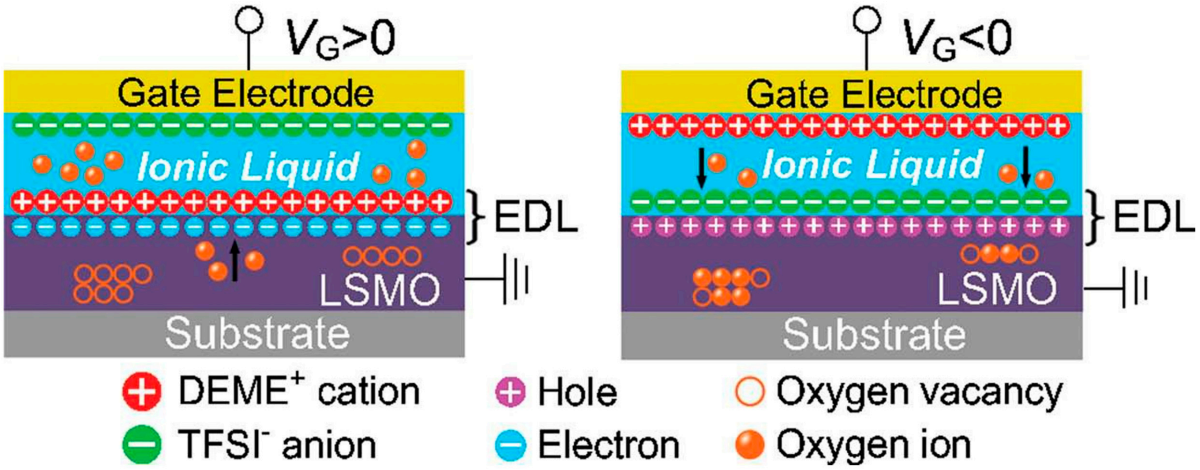

Figure 5. The left and right graphs, respectively, illustrate the schematic structures of the EDL devices using LSMO as the channel material under positive and negative Vg. Reproduced with permission from [57].

The magnetic properties of complex oxides such as $SrFeO_x$ and $SrCoO_{3-x}$ (SCO) can vary with changes in the concentration of O_V [58–60]. In IL-gated $SrFeO_{2.5}/La_{0.7}Sr_{0.3}MnO_3$ and $La_{0.8}Sr_{0.2}CoO_3/La_{0.67}Sr_{0.33}MnO_3$ bilayer systems, by applying a voltage of no more than 3 V, the valence states of Fe^{3+} and Co^{2+} were changed by oxygen migration in the $SrFeO_{2.5}$ and $La_{0.8}Sr_{0.2}CoO_3$ films, respectively, which enable the transformation of $SrFeO_{2.5}$ films between different structures and the reversible toggling of MA between IP and OOP of the $La_{0.67}Sr_{0.33}MnO_3$ layer, both accompanied by changes in interfacial exchange bias at low temperatures (<10 K) [58,59]. In 2021, a reversible phase transition induced by oxygen transport in IL-gated $SrCoO_{3-x}/La_{0.7}Sr_{0.3}MnO_3$ heterojunctions was directly observed using X-ray absorption spectroscopy (XAS). This phase transition occurs between the antiferromagnetic insulating brownmillerite phase (B-SCO, x = 0.5), characterized by ordered O_V, and the ferromagnetic conductive perovskite phase (P-SCO, x = 0), which lacks O_V (Figure 6a) [60]. As shown in Figure 6b, the applied voltages of ±2 V facilitated the non-volatile extraction and injection of O^{2-} in $SrCoO_{3-x}$. After cooling under a magnetic field of 5 T, reversible switching between the exchange spring (the exchange spring effect refers to the phenomenon where the magnetic moments of a hard magnetic material influence the magnetic moment arrangement of an adjacent soft magnetic material through exchange coupling, resulting in a "spring-like" magnetic structure. This configuration enables magnetization reversal under relatively low external magnetic fields, which is macroscopically manifested as a shift in the hysteresis loop along the vertical axis.) and exchange bias was achieved at a low temperature of 5 K. These works not only demonstrate that the exchange bias in oxide bilayer films can be modulated by an electric field but also provide new insights into the formation and annihilation of O_V under the influence

of the EDL [61]. As for magnetic metal heterojunctions, an inserted dielectric layer of HfO_2 can provide an extra oxygen source for modulation. In 2016, Song et al. [62] utilized IL as a gating electrolyte for a Pt/Co/Ni/HfO_2 multilayer structure (Figure 6c). The oxidation states of the Co/Ni interface was modulated by voltage-driven O^{2-} migration at the interface of the HfO_2 and Co/Ni layers, leading to the coupling of an antiferromagnetic CoO/NiO phase with the ferromagnetic Co/Ni phase in the form of an insertion layer. Thus, stable perpendicular exchange bias was established below 200 K. As shown in Figure 6d, the application voltage of +4 V reduced the exchange bias field by 538 Oe, representing a modification of more than fifty percent of the initial value. A similar effect was also achieved in IL-gated Ta/Pt/PtMn/Co/HfO_2 multilayer films, wherein the O^{2-} migration changed the oxidation state of the ferromagnetic Co layer, thereby achieving electric field control of the exchange bias at RT [63].

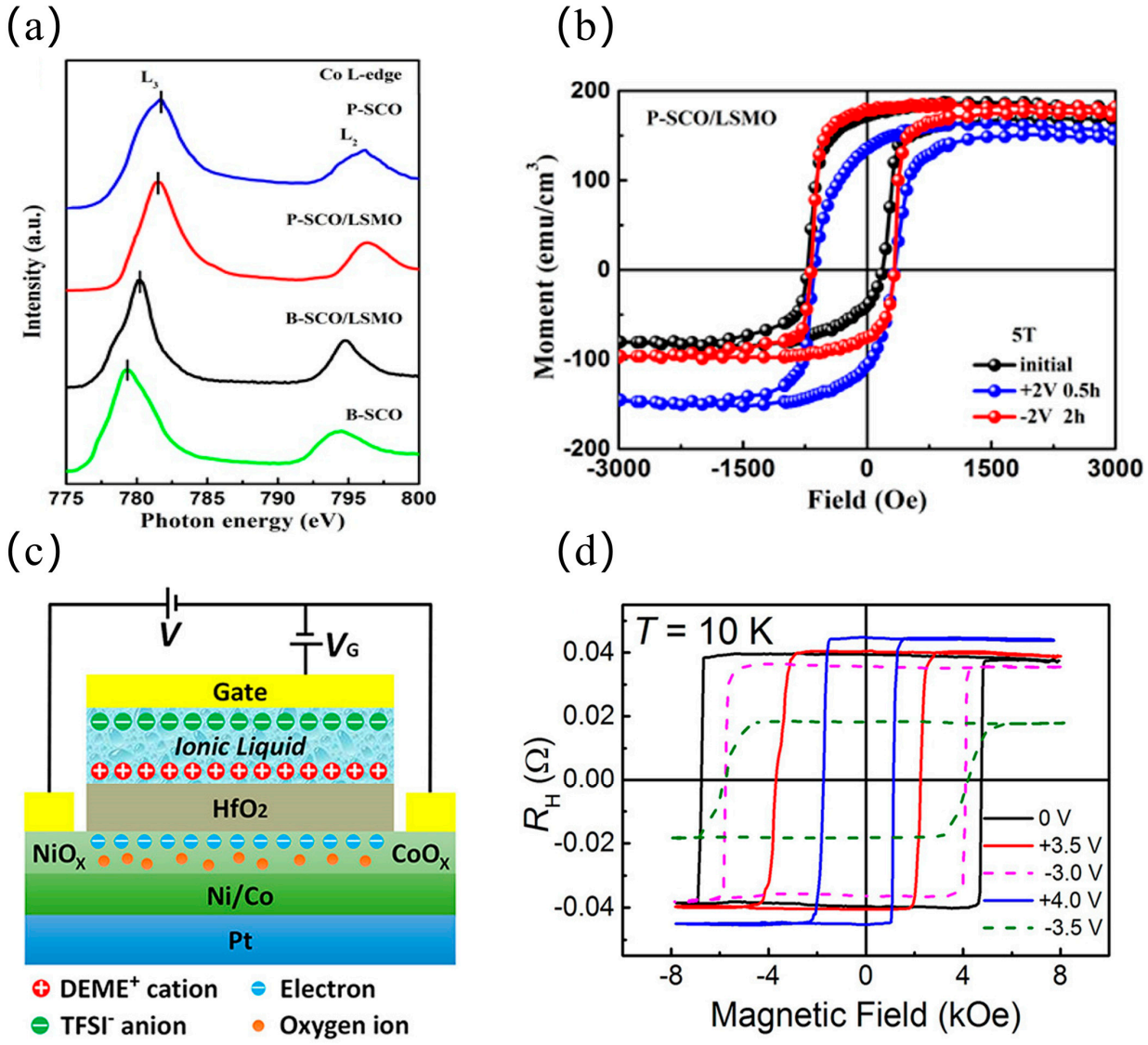

Figure 6. (**a**) The XAS curves of the Co L-edge in the $SrCoO_{3-x}$/LSMO bilayers, where green and blue represent the Co L-edge of B-SCO and P-SCO films, respectively. (**b**) The in-plane minor loop of initial and gated P-SCO/LSMO bilayers measured at 5 K after the positive 5 T cooling field. Reproduced with permission from [60]. (**c**) The schematic representation of the EDL structure established in the Pt/Co/Ni/HfO_2 multilayer films following the application of a positive Vg. (**d**) The anomalous Hall effect (AHE) curves measured under various Vg after field cooling from RT to 10 K. Reproduced with permission from [62].

3.1.2. Resistive Switching Effect

Unlike intrinsically magnetic metal oxides, such as LSMO and SCO, certain oxides in nature (e.g., HfO_2 [64], TiO_2 [65], and ZnO [66]) are not inherently magnetic. However, it is demonstrated that magnetism can be induced by the introduction of O_V in these materials. Resistive switching (RS) effect usually refers to the reversible change in the resistance of certain materials induced by an applied voltage, which triggers ion migration or the formation/breaking of conductive filaments. The resistance toggles between a high-resistance state (HRS) and a low-resistance state (LRS), typically induced by O_V migration or charge accumulation, which exhibits non-volatile characteristics [67,68]. Hu et al. [65,66] used the aforementioned oxides as dielectric layers in combination with resistive random-access memory (RRAM) to obtain. They observed that when the device switched between HRS and LRS under applied voltage, the magnetization of the sample also changed, which is closely related to the concentration of the O_V. Currently, the modulation of exchange bias by electric field-induced RS effects have been observed in several material systems resistive switching memory devices. For example, in the Co/CoO-ZnO/Ag tunnel junction shown in Figure 7a, Li et al. [69] demonstrated that the ferromagnetic phase transition of the CoO_{1-v} (v represents O_V) layer can be controlled by the electric field-driven migration of O^{2-} between insulating CoO_{1-v} and semiconducting ZnO_{1-v}, achieving reversible control of the exchange bias with voltage below 1 V. Song et al. [70] have conducted localized manipulation of the exchange bias field (H_{EB} = 1750 Oe) in $Co/CoO_x/HfO_x/Pt$ (CoO_x/HfO_x represents the composite resistive layer) at temperatures below 10 K (Figure 7b). The RS phenomenon in the heterojunction originates from the formation and rupture of conductive filaments generated by O_V within the CoO_x and HfO_x insulating layers. These researchers suggest the potential for voltage control of exchange bias based on the resistive switching effect at RT. In 2018, Du et al. [71] reported reversible and non-volatile manipulation of the exchange bias at RT in Pt/Co/NiO/Pt heterojunctions by the RS effect. As shown in Figure 7c, the O^{2-} was driven towards the NiO layer interface under a positive voltage. After the break of Ni-O bonds, the generated Ni^{+} diffused towards the interface of the Co cathode. Specific ion movement paths were created when accumulated ions were enough to form a fine conductive nickel filament. The formation of nickel filaments in the NiO layer and rupture near the Co-NiO interface are the fundamental reasons for the resistance switching between HRS and LRS and the modification of the exchange bias field (Figure 7d). In addition, they further investigated the effect of electrochemical metallization-induced RS on the perpendicular exchange bias in Ag/MZO/Pt/FeMn/Co/ITO heterojunctions. The new device exhibited active metallic silver filaments longer than 8 nm at RT, with faster response speed and longer lifespan [72].

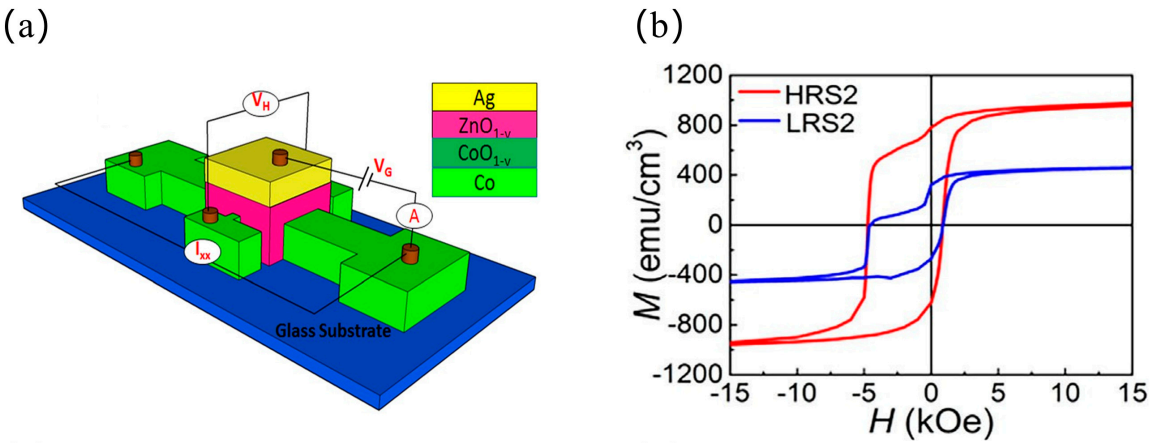

Figure 7. *Cont.*

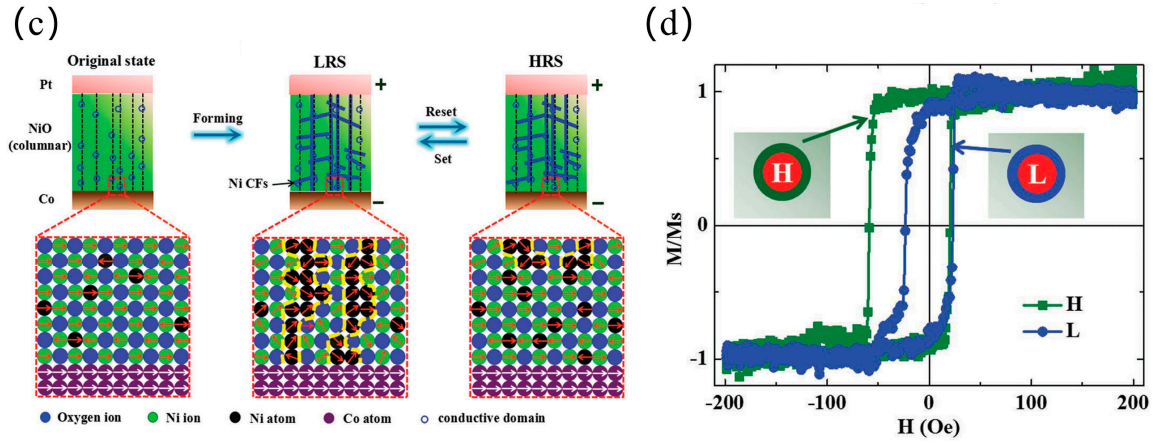

Figure 7. (**a**) Schematic of the Co/CoO-ZnO/Ag tunnel junction device, wherein a CoO_{1-v} layer forms at the interface after the deposition of Co and ZnO_{1-v}. Reproduced with permission from [69]. (**b**) The hysteresis curves of the second HRS and second LRS measured at 10 K after field cooling in the $Co/CoO_x/HfO_x/Pt$ device. Reproduced with permission from [70]. (**c**) The schematic of the Pt/Co/NiO/Pt heterojunction demonstrating reversible toggling among the original state, LRS, and HRS. The magnified region illustrates the magnetic moment alignment of Ni and Co atoms around the NiO-Co interface during nickel filament formation and rupture. (**d**) The schematic shows the M–H loops where the heterojunction is in HRS/LRS. Reproduced with permission from [71].

3.2. Voltage-Controlled Exchange Bias Based on Hydrogen Ions

In 2012, Natelson et al. [73] first observed a significant increase in conductance in IL-gated single-crystal VO_2 nanowires when a positive Vg was applied above the transition temperature. They attributed this change to the electrochemical hydrogen doping of the VO_2, wherein the H^+ generated from the electrolysis of residual water in IL. As the smallest ions, H^+ exhibits distinct advantages like high response speed and long cyclability in VCM. Harnessing this strategy, Yu et al. [74] realized a reversible and non-volatile electric field control of tri-state phase transformation based on the dual ions migration of H^+ and O^{2-} in IL-gated $SrCoO_{2.5}$ thin films, wherein the insulating ferromagnet H-$SrCoO_{2.5}$ phase with novel structure under positive voltage and metallic ferromagnet $SrCoO_{3-x}$ phase with perovskite structure under negative voltage was formed, respectively. Moreover, the decomposition of H_2O can be catalyzed by noble metals, such as Aurum (Au), with the assistance of oxides. Tan and colleagues [35] reported voltage-controlled toggling of MA of the Co layer in an all-solid-state $Pt/Co/GdO_x/Au$ heterostructure. Under the applied voltage, the H_2O absorbed from the surrounding environment was decomposed into H^+ and O^{2-} in the Au layer. After applying a +3 V voltage for 800 s, the H^+ were pumped into the GdO_x layer and then transported to the Co/GdO_x interface. Hydrogen accumulation at the Co/GdO_x interface induces a transformation of MA in the Co film, resulting in a 90° magnetization reversal at RT. These findings have important implications for the regulation of exchange bias by voltage-driven hydrogen migration.

Palladium (Pd) has the remarkable ability to absorb a large volume of hydrogen [36]. Meanwhile, it can induce PMA of the adjacent ferromagnetic layer. These properties make Pd an interesting material for hydrogen storage applications and spintronic device research. In 2021, Zehner et al. [75] realized reversible modulation of the MA and perpendicular exchange bias by voltage-induced H^+ pumping in a $NiO/Pd/Co/Pd/GdO_x/Au$ solid-state heterojunction at RT. The H^+ was driven through hydrated $Gd(OH)_3$ and absorbed at the Pd/Co interface under voltage of no more than 3 V, which induced a 90° toggling of the MA of the ultrathin Co layer, resulting in the ON/OFF of coercivity and the exchange bias field. Additionally, after the first cycle, an increase in coercivity was observed upon returning to the initial state, which can be attributed to the transition of the Pd/Co/Pd

heterojunction from an amorphous to crystalline state. Notably, the insertion of a Pd layer avoided the direct contact of the Co and NiO layer, thereby inhibiting the formation of antiferromagnetic CoO, which is crucial for enhancing the stability of the perpendicular exchange bias. Very recently, in the $GdO_x/Co_{0.8}Ni_{0.2}O/Co$ heterostructure shown in Figure 8a, Beach et al. [76] demonstrated the enhanced perpendicular exchange bias by over 100% in a reversible and analog manner by voltage-driven H^+ migration (Figure 8b,c). This phenomenon serves as an isothermal analog to conventional field-cooling, indicating that small adjustments in the rotatability of AFM grains can lead to considerable changes in the average coupling energy. Utilizing this method, a bidirectionally stable ferromagnet can be rendered unidirectionally stable solely through gate voltage. The research not only offers an approach for dynamically tailoring exchange bias with broad applications for spintronics and neuromorphic computing but also provides new insights into the fundamental mechanism of exchange bias in polycrystalline films.

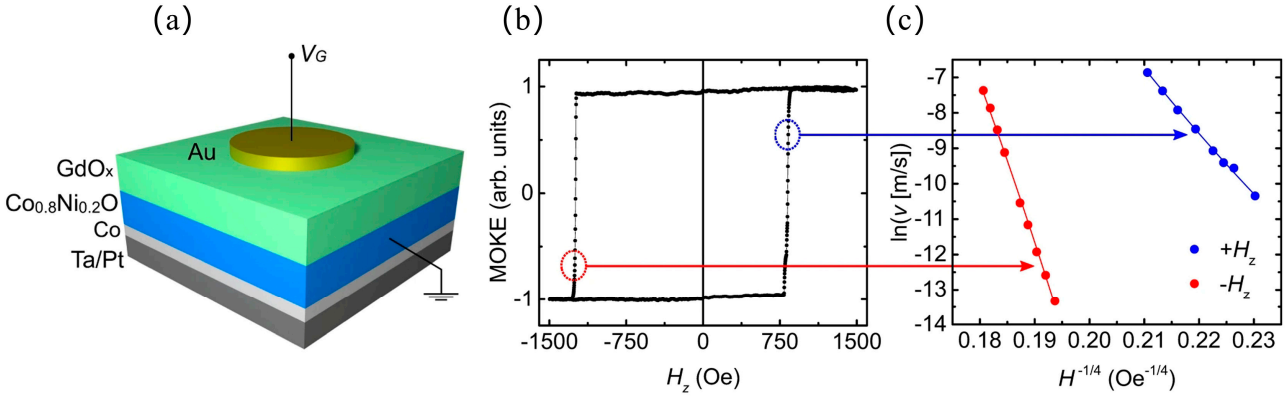

Figure 8. (**a**) Schematic of the $GdO_x/Co_{0.8}Ni_{0.2}O/Co$ heterostructure. (**b**) Hysteresis loop of sample showing exchange bias at 20 K. (**c**) The *lnv* (scanning rate) as a function of $H^{-1/4}$ for sample in (**b**), solid lines show the fit state with $H_E = -229$ Oe. Reproduced with permission from [76].

3.3. Voltage-Controlled Exchange Bias Based on Lithium Ions

In the structure of lithium-ion batteries (LIBs), active materials undergo reversible lithiation/delithiation over thousands of cycles, exhibiting varying degrees of redox reactions depending on the applied potential. The most prevalent reaction process in LIBs is the intercalation reaction, wherein Li^+ ions are inserted into the target material, causing only a minor fraction of the ions in the active material to be reduced or oxidized without significantly altering its crystal structure [34,77]. In contrast to intercalation reactions, conversion reactions are predicated on a complete structural phase transformation characterized by deeper Li^+ penetration and superior reversible lithiation capabilities [33,78]. In recent years, magnetism modulation by electric field-driven Li^+ transport based on LIB structures has achieved many significant results [33,34,77–79]. VCM by Li^+ migration can enable low consumption, fast response speed, and non-volatile and bulk effects at RT. In 2014, by constructing a liquid LIB structure, Hahn et al. [77] achieved efficient and reversible modulation of the magnetism of γ-Fe_2O_3 with thickness in tens of micrometers. The M_S at RT varied by approximately 30% under a voltage of 1.7 V. Later, Wu et al. [33] and Chen et al. [79] realized the VCM of α-Fe_2O_3 and Fe_3O_4, respectively, through Li^+ migration within the LIB structure. The discharge/charge process of the LIB corresponds to the lithiation/delithiation process of the cathode material that is involved with charge transfer. This process not only alters the valence state of transition metals but can also change the crystal lattice and microstructure, enabling high manipulation efficiency.

Concerning exchange bias modulation based on LIB structures, Li et al. [28] reported the voltage control of ON-OFF magnetism and exchange bias via reversible Li^+ migration in Co/CoO bilayers (Figure 9a). Reversible switching of magnetic phase transition between superparamagnetic Co nanoparticles and antiferromagnetic CoO was achieved, ascribed to the redox reaction induced by the intercalation/deintercalation of Li^+ in the cathode material. As shown in Figure 9b, remarkable modulation of the exchange bias at 5 K and reversible tuning of coercivity by 71% and M_S by 118% at RT were demonstrated. In comparison to liquid LIB structures, all-solid-state lithium-ion capacitors are more compatible with modern semiconductor industries. In all-solid-state $LiCoO_2$/LICGC/Co_3O_4/Co heterostructures, Mustafa et al. [80] achieved reversible control of exchange bias at a low temperature of 10 K by voltage-driven Li^+ intercalation/deintercalation in the antiferromagnetic layer Co_3O_4. In another research, they replaced the cathode material in the structure with a NiO/Co bilayer, successfully elevating the operating temperature of the device to RT (Figure 9c) [81]. The modulation mechanism associated with Li^+ migration in Co_3O_4/Co and NiO/Co heterostructures is the same as intercalation/deintercalation. Specifically, due to the existence of the Fermi energy, lithium ions are more compatible with octahedral sites than tetrahedral sites in the lattice [82]. When an electric field drives Li^+ into the antiferromagnetic Co_3O_4 and NiO layer, Li^+ preferentially occupies the octahedral vacancy defects associated with Co^{3+} in Co_3O_4 and Ni^{2+} in NiO, respectively. This will alter the local valence state of target ions as well as the bond lengths and angles of Co-O/Ni-O bonds, creating strain in the Co-O/Ni-O stretching band, affecting interfacial exchange coupling and finally modifying the exchange bias field.

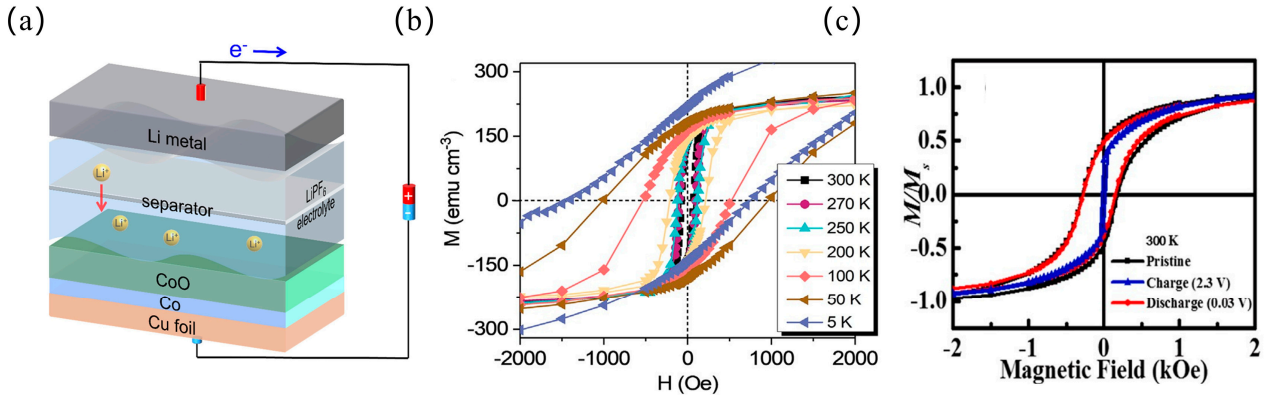

Figure 9. (**a**) Schematic of the LIB structure consisting of CoO/Co bilayer film and electrolyte containing $LiPF_6$. (**b**) The hysteresis curves of CoO/Co bilayer film measured at different temperatures. Reproduced with permission from [28]. (**c**) The normalized hysteresis curve of the device in the pristine state and charge and discharge states at 300 K. Reproduced with permission from [81].

Currently, a new mechanism as interfacial storage was demonstrated theoretically and experimentally, which is used to explain the extra storage capacity of conversion-type electrodes of LIBs [83–85]. This interfacial storage mechanism shows capacitive behavior, which combines the characteristics of LIBs and supercapacitors, exhibiting great superiorities in tuning the magnetism of metals in terms of response speed, lifespan, and modulation amplitude, as depicted in Figure 10. Voltage control of exchange bias upon interfacial storage-modulated magnetism in antiferromagnetic metals is worth further exploration.

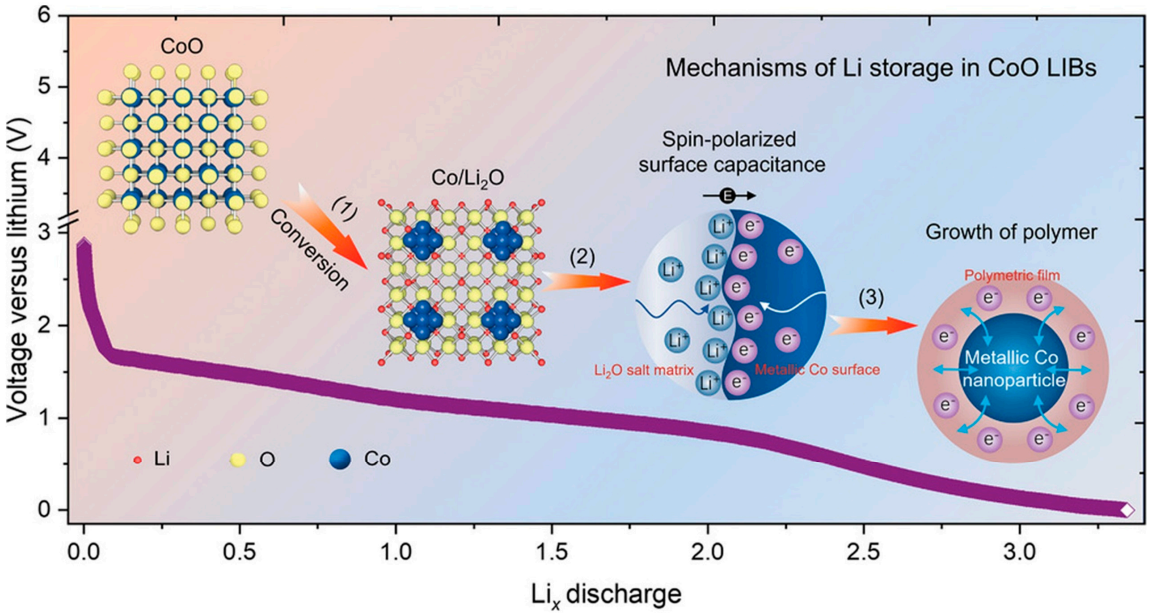

Figure 10. Schematics of extra charge storage mechanism in CoO LIBs. Reproduced with permission from [84].

3.4. Voltage-Controlled Exchange Bias Based on Emerging New Ions

With the continuous development of the magneto-ionic mechanism and the maturation of related devices, emerging new ions, such as fluoride (F^-) and nitrogen (N^{3-}), have exhibited distinct advantages in the modulation of the magnetism of materials. In recent years, advances in electrochemical energy storage have facilitated the search for new charge-transfer ions. Compared to the well-established LIB technology, F^- can form stable fluorides with various transition metals, offering more options for the design of cathode and anode materials [86,87]. In addition, fluoride-ion batteries (FIBs) feature a theoretical energy density exceeding 5000 Wh/L, potentially achieving several times the energy storage capacity of LIBs. Unlike Li^+, F^- can only enter target materials through intercalation/deintercalation reactions and has not yet demonstrated more complex mechanisms such as conversion reactions, with perovskite-related structures being the most notable examples [88,89]. Clemens et al. [37] first demonstrated electric field-driven F^- migration to achieve reversible and effective manipulation of magnetism in $La_{1.3}Sr_{1.7}Mn_2O_7$. When voltage was applied at 10 K, the oxygen vacancy defects in $La_{1.3}Sr_{1.7}Mn_2O_7$ were occupied by the intercalated F^- ions, forming a new fluorinated phase, $La_{1.3}Sr_{1.7}Mn_2O_7F_{1-x}$. Significant modification in M_S up to 67% was realized, comparable to the optimal results obtained based on LIB structures but with a lower operating voltage below 1 V (Li-ion intercalation ≈ 2 V), thus demonstrating higher magnetoelectric coupling efficiency. In 2022, Gupta et al. [90] found that the injection of F^- induces a transformation of Fe into antiferromagnetic FeF_2 in Si/Al/Fe/Fe^{57}/Fe metal multilayers at RT. By examining the evolution of magnetization and magnetic domain structure of films subjected to varying flux of F^-, it is found that the exchange bias field changes with the reduction in disorder at the Fe/FeF_2 interface as F^- flux increases. This experiment did not involve voltage-driven processes; further exploration of voltage control of exchange bias based on F^- migration is needed.

In addition, Sort et al. [38,91] have demonstrated that nitrogen exhibits significant advantages over its oxygen-based counterparts in terms of both energy and functionality, while maintaining compatibility with current complementary metal-oxide-semiconductor (CMOS) technology. The impact of N^{3-} migration on the exchange bias has also attracted

the interest of researchers. Quarterman et al. [92] have demonstrated that the N^{3-} can be diffused from the MnN layer to the Ta layer in Ta/MnN/CoFeB heterojunctions through annealing, resulting in nitrogen vacancies in the MnN layer. This process induces the migration of Co and Fe from the ferromagnetic layer into the MnN layer, forming a mixed interface and consequently reducing the in-plane exchange bias field of the system. This finding suggests that N^{3-} can serve as a potential magnetic ion for modulating exchange bias. In 2023, as shown in Figure 11a, Liu et al. [93] reported that voltage-driven N^{3-} migration significantly enhances the exchange bias in Ta/MnN/$Co_{0.7}Fe_{0.3}$/Ta heterostructures. After field cooling, N^{3-} diffused from the MnN layer to the Ta layer, resulting in significant exchange bias fields of 1484 Oe at 10 K (Figure 11b) and 618 Oe at 300 K (Figure 11c). Upon adjusting the voltage, the exchange bias field can be further enhanced by 19% and 5%, respectively. Very recently, Sort et al. [94] demonstrated that applying a Vg without thermal annealing in Ta/$Co_xMn_{1-x}N$/Ta metal films can result in a non-volatile increase in the MA by over 100% at RT and regulate the exchange bias field at low temperatures. The results showed that adding Co to MnN reduces the Mn-N bond energy, with the effect increasing as the Co content increases. When x = 0.55, applying a positive voltage of 20 V, the MA of the sample increased from 15.1 emu/cm³ to 31.9 emu/cm³. Upon cooling below 30 K, the system exhibited an exchange bias effect, with a modulation amplitude reaching up to 50% at 10 K. This regulation mechanism is attributed to the formation of an FM/AFM mixed phase in the $Co_xMn_{1-x}N$ layer after Co doping. When N^{3-} migrates to the Ta layer under the electric field, the proportion of the AFM phase will decrease.

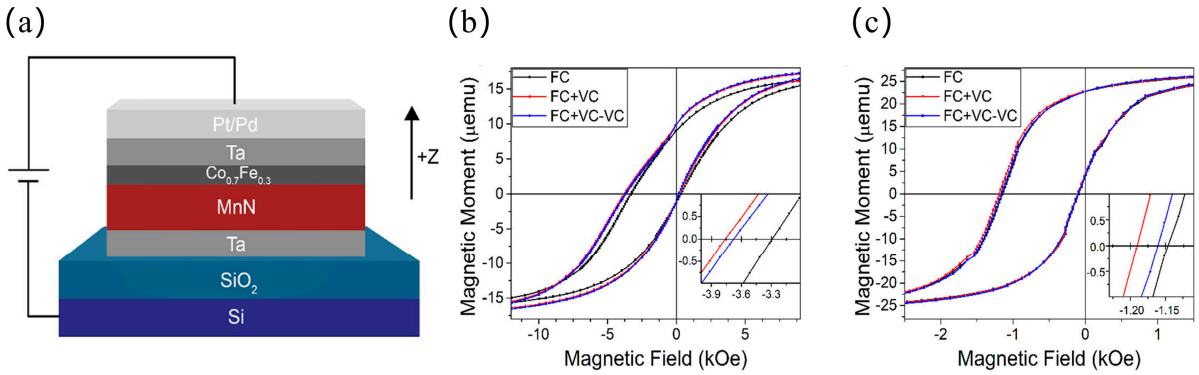

Figure 11. (**a**) The schematic diagram of Ta/MnN/$Co_{0.7}Fe_{0.3}$/Ta heterostructure is depicted with a positive Vg applied. The arrow indicates the Z-axis. (**b**) Hysteresis curve of the sample at 10 K. (**c**) Hysteresis curve of the sample at 300 K. Each measurement was taken after preparing the same sample in the FC, FC+VC, and FC+VC-VC states. Reproduced with permission from [93].

4. Comparison of Magneto-Ionic Mechanisms Based on Different Ions

Although many significant achievements have been made in the field of voltage control of exchange bias based on magnet-ionic mechanisms, further exploration and optimization in terms of device structure, underlying mechanisms, and performance metrics remain key research issues. In this section, we will give a brief comparison of the modulation effects in terms of operating temperature, response time, voltage range, and modulating amplitude of exchange bias. To facilitate comparison, representative studies of voltage-controlled exchange bias are presented in Table 1.

Table 1. Comparison of exchange bias controlled by different magneto-ionic mechanisms.

System	Ions	T (K)	Response Time	Voltage Range (V)	Change in H_{EB} (Oe)	Reversibility	Ref.
$Gd/Ni_{0.33}Co_{0.67}O$	O^{2-}	300	\(No data)	20	28	reversible	[52]
$Gd/Ni_{0.33}Co_{0.67}O$	O^{2-}, He^{+}	300	\	\	\	irreversible	[53]
$SrFeO_{2.5}/La_{0.7}Sr_{0.3}MnO_3$	O^{2-}	10	45 min	−2~+0.7	135	reversible	[58]
$La_{0.8}Sr_{0.2}CoO_3/La_{0.67}Sr_{0.33}MnO_3$	O^{2-}	5	1~5 min	−2.7~+3	203/555	reversible	[59]
$SrCoO_{3-x}/La_{0.7}Sr_{0.3}MnO_3$	O^{2-}	5	0.5 h/2 h	±2	\	reversible	[60]
$Pt/[Co/Ni]_N/HfO_2$	O^{2-}	10	10~60 min	−3.5~+4	538	reversible	[62]
$Ta/Pt/PtMn/Co/HfO_2$	O^{2-}	300	5 min/10 min	−2.7~+3.7	\	reversible	[63]
Co/CoO-ZnO/Ag	O^{2-}	5	\	±1	503	reversible	[69]
$Co/CoO_x/HfO_x/Pt$	O^{2-}	10	\	−1.3~+3.3	\	reversible	[70]
Pt/Co/NiO/Pt	O^{2-}	300	105s (keep)	1.4~4.3	19.1	reversible	[71]
Ag/MZO/Pt/FeMn/Co/ITO	O^{2-}	300	104s (keep)	±1	15	reversible	[72]
$NiO/Pd/Co/Pd/GdO_x/Au$	H^{+}	300	0~176 s	3	68	reversible	[75]
$Co/Co_{0.8}Ni_{0.2}O$	H^{+}	300	<1 ms	0~14	38	reversible	[76]
$Li/LiPF_6/CoO/Co/Cu$	Li^{+}	5	80~180 min	0~3	670.1	reversible	[28]
$LiCoO_2/LICGC/Co_3O_4/Co$	Li^{+}	10	\	0.03~1.6	249	reversible	[80]
$LiCoO_2/LICGC/NiO/Co$	Li^{+}	300	\	0.03~2.3	20	reversible	[81]
$Si/Al/Fe/Fe^{57}/Fe$	F^{-}	300	\	\	48.3	irreversible	[90]
$Ta/MnN/Co_{0.7}Fe_{0.3}/Ta$	N^{3-}	300/10	1 h	20	285/28	reversible	[93]
$Ta/Co_xMn_{1-x}N/Ta$	N^{3-}	10	1 h	20	670	reversible	[94]

Concerning operation temperature, FM/AFM material systems with a blocking temperature above RT are a precondition to achieve exchange bias modulation at RT [52,53,63,71,72,75,76,81,93]. In addition, the mechanism of the reaction also affects the blocking temperature. For example, in Co/CoO bilayers, the insertion/extraction of Li^{+} results in conversion reactions of CoO, transforming the particle sizes of CoO film into much smaller ones, which significantly reduce the blocking temperature of the exchange bias in the Co/CoO bilayer, as the exchange bias of bilayers has a strong relationship with the particle size of the films [28,80]. In terms of response speed, the tuning effect based on O^{2-} has a relatively long response time due to the high diffusion energy barrier of O^{2-}, while a surface effect has a much shorter response time in the order of seconds [58–60,62,63]. H^{+} has the fastest response speed in the order of milliseconds, taking advantage of its smallest ionic size [76]. It is obvious that the response time and applied voltage range is strongly correlated with the size of the migrated ions. The exception is Li^{+}, which can achieve a significant modification of the exchange bias due to its bulk effect while needing a relatively long response time [28]. The reversibility of the exchange bias modulation based on the magneto-ionic mechanism is not an issue; however, the cyclability needs to be taken into account to meet the requirements of practical applications [71,72].

To sum up, voltage-controlled exchange bias based on each type of magnetic ion has its unique advantages. In addition, there is often a trade-off between the operating temperature, response time, applied voltage range, and tuning amplitude. Take LIB structure devices as an example; charging/discharging at low rates can obtain a more comprehensive Li^{+} intercalation effect but at the expense of response speed. On the contrary, charging/discharging at high rates achieves a faster response speed but at the expense of cycle stability. It is necessary to obtain a balance between various parameters and select suitable ions to meet the practical requirements [85].

5. Conclusions

This review introduces the recent progress in electric field control of exchange bias based on magneto-ionic mechanisms. From the perspective of ion species associated with magneto-ionic mechanisms, the material systems, underlying mechanisms, and performance metrics of representative works in the development process were presented and discussed. Magnetoelectric coupling based on ions migration provides dynamic and non-volatile exchange bias regulation, which has shown great advantages in driving the development of high-speed, low-energy, non-volatile spintronics devices.

Despite its potential applications, the field still faces several challenges: (1) Modulations based on O^{2-} are constrained by their inherent redox reaction rates, resulting in slower response times, typically requiring several minutes to tens of minutes, with most reactions achieving exchange bias modulation only at low temperatures. (2) Currently, most gate electrolytes are liquid, which are difficult to integrate with modern CMOS technology and effectively control device dimensions. (3) Hydrogen-based exchange bias modification exhibits the state-of-the-art response time (millisecond orders) and long lifespan (hundreds to thousands of cycles), which is still far from meeting the practical demands of modern spintronic devices. (4) Emerging new ions, such as fluorine and nitrogen, maintain compatibility with current CMOS technology. Clarifying the underlying reaction mechanisms and establishing a comprehensive set of material and device design principles to further enhance ion migration efficiency is crucial.

The continuous advancement of electrochemical energy storage devices presents new opportunities for both fundamental research and practical applications in the field of voltage-controlled exchange bias. Selecting target electrode materials with faster ion migration pathways and exploring electrolytes with higher ion mobility are optimal solutions for improving the performance of voltage-controlled exchange bias. The development of fundamental mechanisms and practical applications in electrochemical energy storage devices, such the interfacial storage mechanism for LIBs, offers promising new approaches for the voltage control of exchange bias [83,84].

Author Contributions: Conceptualization, Y.L. (Yifu Luo); writing, Y.L. (Yifu Luo); writing—review and editing, S.L., Y.L. (Yuxin Li), Z.W. and J.Z.; supervision, L.Z.; funding acquisition, J.Z. All authors have read and agreed to the published version of the manuscript.

Funding: This work was funded by the Youth Science and Technology Project of the Chongqing Municipal Education Commission (KJQN2024005) and the Natural Science Foundation of the Chongqing Municipal Science and Technology Bureau (Grant No. CSTB2022NSCQ-MSX0898).

Data Availability Statement: The original contributions presented in this study are included in the article.

Conflicts of Interest: The authors declare no conflicts of interest.

References

1. Wolf, S.A.; Awschalom, D.D.; Buhrman, R.A.; Daughton, J.M.; von Molnár, S.; Roukes, M.L.; Chtchelkanova, A.Y.; Treger, D.M. Spintronics: A spin-based electronics vision for the future. *Science* **2001**, *294*, 1488–1495. [CrossRef]
2. Žutić, I.; Fabian, J.; Sarma, S.D. Spintronics: Fundamentals and applications. *Rev. Mod. Phys.* **2004**, *76*, 323–410. [CrossRef]
3. Song, C.; Cui, B.; Li, F.; Zhou, X.; Pan, F. Recent progress in voltage control of magnetism: Materials, mechanisms, and performance. *Prog. Mater. Sci.* **2017**, *87*, 33–82. [CrossRef]
4. Nogués, J.; Schuller, I.K. Exchange bias. *J. Magn. Magn. Mater.* **1999**, *192*, 203–232. [CrossRef]
5. Manna, P.K.; Yusuf, S.M. Two interface effects: Exchange bias and magnetic proximity. *Phys. Rep.* **2014**, *535*, 61–99. [CrossRef]
6. Grünberg, P.A. Exchange anisotropy, interlayer exchange coupling and GMR in research and application. *Sens. Actuators A Phys.* **2001**, *91*, 153–160. [CrossRef]

7. Takagishi, M.; Koi, K.; Yoshikawa, M.; Funayama, T.; Iwasaki, H.; Sahashi, M. The applicability of CPP-GMR heads for magnetic recording. *IEEE Trans. Magn.* **2002**, *38*, 2277–2282. [CrossRef]
8. Yang, Q.; Zhou, Z.; Sun, N.X.; Liu, M. Perspectives of voltage control for magnetic exchange bias in multiferroic heterostructures. *Phys. Lett. A* **2017**, *381*, 1213–1222. [CrossRef]
9. Ramesh, R.; Martin, L.W. Electric field control of magnetism: Multiferroics and magnetoelectrics. *Riv. Nuovo Cimento* **2021**, *44*, 251–289. [CrossRef]
10. Gradauskaite, E.; Meisenheimer, P.; Müller, M.; Heron, J.; Trassin, M. Multiferroic heterostructures for spintronics. *Phys. Sci. Rev.* **2021**, *6*, 20190072. [CrossRef]
11. He, X.; Wang, Y.; Wu, N.; Caruso, A.N.; Vescovo, E.; Belashchenko, K.D.; Dowben, P.A.; Binek, C. Robust isothermal electric control of exchange bias at room temperature. *Nat. Mater.* **2010**, *9*, 579–585. [CrossRef]
12. Borisov, P.; Hochstrat, A.; Chen, X.; Kleemann, W.; Binek, C. Magnetoelectric switching of exchange bias. *Phys. Rev. Lett.* **2005**, *94*, 117203. [CrossRef]
13. Chen, X.; Hochstrat, A.; Borisov, P.; Kleemann, W. Magnetoelectric exchange bias systems in spintronics. *Appl. Phys. Lett.* **2006**, *89*, 202508. [CrossRef]
14. Laukhin, V.; Skumryev, V.; Martí, X.; Hrabovsky, D.; Sánchez, F.; García-Cuenca, M.V.; Ferrater, C.; Varela, M.; Lüders, U.; Bobo, J.F.; et al. Electric-field control of exchange bias in multiferroic epitaxial heterostructures. *Phys. Rev. Lett.* **2006**, *97*, 227201. [CrossRef] [PubMed]
15. Wu, S.; Cybart, S.A.; Yu, P.; Rossell, M.; Zhang, J.; Ramesh, R.; Dynes, R. Reversible electric control of exchange bias in a multiferroic field-effect device. *Nat. Mater.* **2010**, *9*, 756–761. [CrossRef] [PubMed]
16. Wu, S.M.; Cybart, S.A.; Yu, P.; Rossell, M.D.; Zhang, J.X.; Ramesh, R.; Dynes, R.C. Full electric control of exchange bias. *Phys. Rev. Lett.* **2013**, *110*, 067202. [CrossRef] [PubMed]
17. Heron, J.T.; Trassin, M.; Ashraf, K.; Gajek, M.; He, Q.; Yang, S.Y.; Nikonov, D.E.; Chu, Y.H.; Salahuddin, S.; Ramesh, R. Electric-field-induced magnetization reversal in a ferromagnet-multiferroic heterostructure. *Phys. Rev. Lett.* **2011**, *107*, 217202. [CrossRef]
18. Polisetty, S.; Echtenkamp, W.; Jones, K.; He, X.; Sahoo, S.; Binek, C. Piezoelectric tuning of exchange bias in a $BaTiO_3$/Co/CoO heterostructure. *Phys. Rev. B Condens. Matter Mater. Phys.* **2010**, *82*, 134419. [CrossRef]
19. Chen, A.; Zhao, Y.; Li, P.; Zhang, X.; Peng, R.; Huang, H.; Zou, L.; Zheng, X.; Zhang, S.; Miao, P.; et al. Angular dependence of exchange bias and magnetization reversal controlled by electric-field-induced competing anisotropies. *Adv. Mater.* **2015**, *28*, 363–369. [CrossRef]
20. Wang, Y.; Zhou, X.; Song, C.; Yan, Y.; Zhou, S.; Wang, G.; Chen, C.; Zeng, F.; Pan, F. Electrical control of the exchange spring in antiferromagnetic metals. *Adv. Mater.* **2015**, *27*, 3196–3201. [CrossRef] [PubMed]
21. Zhang, P.; Yin, G.; Wang, Y.; Cui, B.; Pan, F.; Song, C. Electrical control of antiferromagnetic metal up to 15 nm. *Sci. China Phys. Mech. Astron.* **2016**, *59*, 1–5. [CrossRef]
22. Yang, Q.; Hu, Z.; Zhang, Y.; Su, W.; Cheng, Y.; Peng, B.; Wu, J.; Zhou, Z.; He, Y.; Cui, W.; et al. Voltage control of perpendicular exchange bias in multiferroic heterostructures. *Adv. Electron. Mater.* **2019**, *5*, 1900192. [CrossRef]
23. Bauer, U.; Yao, L.; Tan, A.J.; Agrawal, P.; Emori, S.; Tuller, H.L.; Van Dijken, S.; Beach, G.S. Magneto-ionic control of interfacial magnetism. *Nat. Mater.* **2015**, *14*, 174–181. [CrossRef] [PubMed]
24. Gilbert, D.A.; Grutter, A.J.; Arenholz, E.; Liu, K.; Kirby, B.J.; Borchers, J.A.; Maranville, B.B. Structural and magnetic depth profiles of magneto-ionic heterostructures beyond the interface limit. *Nat. Commun.* **2016**, *7*, 12264. [CrossRef]
25. Bi, C.; Liu, Y.; Newhouse-Illige, T.; Xu, M.; Rosales, M.; Freeland, J.W.; Mryasov, O.; Zhang, S.; te Velthuis, S.G.; Wang, W.G. Reversible control of Co magnetism by voltage-induced oxidation. *Phys. Rev. Lett.* **2014**, *113*, 267202. [CrossRef] [PubMed]
26. Lee, K.Y.; Jo, S.; Tan, A.J.; Huang, M.; Choi, D.; Park, J.H.; Ji, H.I.; Son, J.W.; Chang, J.; Beach, G.S.; et al. Fast magneto-ionic switching of interface anisotropy using yttria-stabilized zirconia gate oxide. *Nano Lett.* **2020**, *20*, 3435–3441. [CrossRef] [PubMed]
27. Li, H.B.; Lu, N.; Zhang, Q.; Wang, Y.; Feng, D.; Chen, T.; Yang, S.; Duan, Z.; Li, Z.; Shi, Y.; et al. Electric-field control of ferromagnetism through oxygen ion gating. *Nat. Commun.* **2017**, *8*, 2156. [CrossRef] [PubMed]
28. Li, Z.; Zhao, Z.; Shang, X.; Zhang, J.; Cai, L.; Pan, Y.; Li, Q.; Li, H.; Cao, Q.; Li, Q. Electrical control of ON-OFF magnetism and exchange bias via reversible ionic motion. *Appl. Phys. Lett.* **2022**, *120*, 082405. [CrossRef]
29. Chen, X.; Wang, K.Y.; Wu, Z.L.; Jiang, S.L.; Yang, G.; Liu, Y.; Teng, J.; Yu, G.H. Interfacial electronic structure-modulated magnetic anisotropy in Ta/CoFeB/MgO/Ta multilayers. *Appl. Phys. Lett.* **2014**, *105*, 092402. [CrossRef]
30. Chen, X.; Feng, C.; Long Wu, Z.; Yang, F.; Liu, Y.; Jiang, S.; Hua Li, M.; Hua Yu, G. Interfacial oxygen migration and its effect on the magnetic anisotropy in Pt/Co/MgO/Pt films. *Appl. Phys. Lett.* **2014**, *104*, 052413. [CrossRef]
31. Yan, Y.N.; Zhou, X.J.; Li, F.; Cui, B.; Wang, Y.Y.; Wang, G.Y.; Pan, F.; Song, C. Electrical control of Co/Ni magnetism adjacent to gate oxides with low oxygen ion mobility. *Appl. Phys. Lett.* **2015**, *107*, 122407. [CrossRef]
32. Zhu, X.; Zhou, J.; Chen, L.; Guo, S.; Liu, G.; Li, R.W.; Lu, W.D. In situ nanoscale electric field control of magnetism by nanoionics. *Adv. Mater.* **2016**, *28*, 7658–7665. [CrossRef]

33. Zhang, Q.; Luo, X.; Wang, L.; Zhang, L.; Khalid, B.; Gong, J.; Wu, H. Lithium-ion battery cycling for magnetism control. *Nano Lett.* **2016**, *16*, 583–587. [CrossRef] [PubMed]
34. Dasgupta, S.; Das, B.; Li, Q.; Wang, D.; Baby, T.T.; Indris, S.; Knapp, M.; Ehrenberg, H.; Fink, K.; Kruk, R.; et al. Toward on-and-off magnetism: Reversible electrochemistry to control magnetic phase transitions in spinel ferrites. *Adv. Funct. Mater.* **2016**, *26*, 7507–7515. [CrossRef]
35. Tan, A.J.; Huang, M.; Sheffels, S.; Büttner, F.; Kim, S.; Hunt, A.H.; Waluyo, I.; Tuller, H.L.; Beach, G.S.D. Hydration of gadolinium oxide (GdO_x) and its effect on voltage-induced Co oxidation in a Pt/Co/GdO_x/Au heterostructure. *Phys. Rev. Mater.* **2019**, *3*, 064408. [CrossRef]
36. Tan, A.J.; Huang, M.; Avci, C.O.; Büttner, F.; Mann, M.; Hu, W.; Mazzoli, C.; Wilkins, S.; Tuller, H.L.; Beach, G.S.D. Magneto-ionic control of magnetism using a solid-state proton pump. *Nat. Mater.* **2019**, *18*, 35–41. [CrossRef] [PubMed]
37. Vasala, S.; Jakob, A.; Wissel, K.; Waidha, A.I.; Alff, L.; Clemens, O. Reversible tuning of magnetization in a ferromagnetic Ruddlesden-Popper-type manganite by electrochemical fluoride-ion intercalation. *Adv. Electron. Mater.* **2020**, *6*, 1900974. [CrossRef]
38. De Rojas, J.; Quintana, A.; Lopeandía, A.; Salguero, J.; Muñiz, B.; Ibrahim, F.; Chshiev, M.; Nicolenco, A.; Liedke, M.O.; Butterling, M.; et al. Voltage-driven motion of nitrogen ions: A new paradigm for magneto-ionics. *Nat. Commun.* **2020**, *11*, 5871. [CrossRef] [PubMed]
39. Chen, G.; Mascaraque, A.; Jia, H.; Zimmermann, B.; Robertson, M.; Conte, R.L.; Hoffmann, M.; González Barrio, M.A.; Ding, H.; Wiesendanger, R.; et al. Large Dzyaloshinskii-Moriya interaction induced by chemisorbed oxygen on a ferromagnet surface. *Sci. Adv.* **2020**, *6*, eaba4924. [CrossRef]
40. Chen, G.; Robertson, M.; Hoffmann, M.; Ophus, C.; Fernandes Cauduro, A.L.; Lo Conte, R.; Ding, H.; Wiesendanger, R.; Blügel, S.; Schmid, A.K.; et al. Observation of hydrogen-induced Dzyaloshinskii-Moriya interaction and reversible switching of magnetic chirality. *Phys. Rev. X* **2021**, *11*, 021015. [CrossRef]
41. Leistner, K. Electrochemical approaches to room temperature magnetoelectric materials. *Curr. Opin. Electrochem.* **2021**, *25*, 100636. [CrossRef]
42. De Rojas, J.; Quintana, A.; Rius, G.; Stefani, C.; Domingo, N.; Costa-Krämer, J.L.; Menéndez, E.; Sort, J. Voltage control of magnetism with magneto-ionic approaches: Beyond voltage-driven oxygen ion migration. *Appl. Phys. Lett.* **2022**, *120*, 070501. [CrossRef]
43. Navarro-Senent, C.; Quintana, A.; Menéndez, E.; Pellicer, E.; Sort, J. Electrolyte-gated magnetoelectric actuation: Materials, mechanisms, and prospective applications. *APL Mater.* **2019**, *7*, 030701. [CrossRef]
44. Gu, Y.; Song, C.; Wang, Q.; Hu, W.; Liu, W.; Pan, F.; Zhang, Z. Emerging opportunities for voltage-driven magneto-ionic control in ferroic heterostructures. *APL Mater.* **2021**, *9*, 040904. [CrossRef]
45. Meiklejohn, W.H.; Bean, C.P. New magnetic anisotropy. *Phys. Rev.* **1956**, *102*, 1413–1414. [CrossRef]
46. Dieny, B.; Speriosu, V.S.; Metin, S.; Parkin, S.S.; Gurney, B.A.; Baumgart, P.; Wilhoit, D.R. Magnetotransport properties of magnetically soft spin-valve structures. *J. Appl. Phys.* **1991**, *69*, 4774–4779. [CrossRef]
47. Meiklejohn, W.H.; Bean, C.P. New magnetic anisotropy. *Phys. Rev.* **1957**, *105*, 904–913. [CrossRef]
48. Mauri, D.; Siegmann, H.C.; Bagus, P.S.; Kay, E. Simple model for thin ferromagnetic films exchange coupled to an antiferromagnetic substrate. *J. Appl. Phys.* **1987**, *62*, 3047–3049. [CrossRef]
49. Malozemoff, A.P. Random-field model of exchange anisotropy at rough ferromagnetic-antiferromagnetic interfaces. *Phys. Rev. B* **1987**, *35*, 3679–3682. [CrossRef]
50. Stamps, R.L. Mechanisms for exchange bias. *J. Phys. D Appl. Phys.* **2000**, *33*, R247–R268. [CrossRef]
51. Gilbert, D.A.; Olamit, J.; Dumas, R.K.; Kirby, B.J.; Grutter, A.J.; Maranville, B.B.; Arenholz, E.; Borchers, J.A.; Liu, K. Controllable positive exchange bias via redox-driven oxygen migration. *Nat. Commun.* **2016**, *7*, 11050. [CrossRef]
52. Murray, P.D.; Jensen, C.J.; Quintana, A.; Zhang, J.; Zhang, X.; Grutter, A.J.; Kirby, B.J.; Liu, K. Electrically enhanced exchange bias via solid-state magneto-ionics. *ACS Appl. Mater. Interfaces* **2021**, *13*, 38916–38922. [CrossRef]
53. Jensen, C.J.; Quintana, A.; Sall, M.; Diez, L.H.; Zhang, J.; Zhang, X.; Ravelosona, D.; Liu, K. Ion irradiation and implantation modifications of magneto-ionically induced exchange bias in Gd/NiCoO. *J. Magn. Magn. Mater.* **2021**, *540*, 168479. [CrossRef]
54. Jeong, J.; Aetukuri, N.; Graf, T.; Schladt, T.D.; Samant, M.G.; Parkin, S.S. Suppression of metal-insulator transition in VO_2 by electric field-induced oxygen vacancy formation. *Science* **2013**, *339*, 1402–1405. [CrossRef] [PubMed]
55. Cui, B.; Song, C.; Wang, G.; Yan, Y.; Peng, J.; Miao, J.; Mao, H.; Li, F.; Chen, C.; Zeng, F.; et al. Reversible ferromagnetic phase transition in electrode-gated manganites. *Adv. Funct. Mater.* **2014**, *24*, 7233–7240. [CrossRef]
56. Cui, B.; Song, C.; Gehring, G.A.; Li, F.; Wang, G.; Chen, C.; Peng, J.; Mao, H.; Zeng, F.; Pan, F. Electrical manipulation of orbital occupancy and magnetic anisotropy in manganites. *Adv. Funct. Mater.* **2014**, *25*, 864–870. [CrossRef]
57. Cui, B.; Song, C.; Mao, H.; Yan, Y.; Li, F.; Gao, S.; Peng, J.; Zeng, F.; Pan, F. Manipulation of electric field effect by orbital switch. *Adv. Funct. Mater.* **2015**, *26*, 753–759. [CrossRef]

58. Saleem, M.S.; Cui, B.; Song, C.; Sun, Y.; Gu, Y.; Zhang, R.; Fayaz, M.U.; Zhou, X.; Werner, P.; Parkin, S.S.; et al. Electric field control of phase transition and tunable resistive switching in $SrFeO_{2.5}$. *ACS Appl. Mater. Interfaces* **2019**, *11*, 6581–6588. [CrossRef]
59. Song, J.; Chen, Y.; Chen, X.; Khan, T.; Han, F.; Zhang, J.; Huang, H.; Zhang, H.; Shi, W.; Qi, S.; et al. Electric Tuning of Magnetic Anisotropy and Exchange Bias of $La_{0.8}Sr_{0.2}CoO_3/La_{0.6}7Sr_{0.33}MnO_3$ Bilayer Films. *Phys. Rev. Appl.* **2020**, *14*, 024062. [CrossRef]
60. Ji, H.; Zhou, G.; Wang, X.; Zhang, J.; Kang, P.; Xu, X. Electric-field reversible switching of the exchange spring and exchange bias effect in $SrCoO_{3-x}/La_{0.7}Sr_{0.3}MnO_3$ heterostructures. *ACS Appl. Mater. Interfaces* **2021**, *13*, 15774–15782. [CrossRef]
61. Zhao, X.W.; Ng, S.M.; Wong, L.W.; Wong, H.F.; Liu, Y.K.; Cheng, W.F.; Mak, C.L.; Zhao, J.; Leung, C.W. Ionic liquid modulation of exchange bias in epitaxial $LaMnO_3$ thin films. *Appl. Phys. Lett.* **2022**, *121*, 162406. [CrossRef]
62. Zhou, X.; Yan, Y.; Jiang, M.; Cui, B.; Pan, F.; Song, C. Role of oxygen ion migration in the electrical control of magnetism in $Pt/Co/Ni/HfO_2$ films. *J. Phys. Chem. C* **2016**, *120*, 1633–1639. [CrossRef]
63. Bednarz, B.; Syskaki, M.A.; Pachat, R.; Prädel, L.; Wortmann, M.; Kuschel, T.; Ono, S.; Kläui, M.; Herrera Diez, L.; Jakob, G. Stabilizing perpendicular magnetic anisotropy with strong exchange bias in PtMn/Co by magneto-ionics. *Appl. Phys. Lett.* **2024**, *124*, 232403. [CrossRef]
64. Lin, Y.; Zeng, F.; Tang, S.; Liu, H.; Chen, C.; Gao, S.; Wang, Y.; Pan, F. Resistive switching mechanisms relating to oxygen vacancies migration in both interfaces in $Ti/HfO_x/Pt$ memory devices. *J. Appl. Phys.* **2013**, *113*, 064510. [CrossRef]
65. Ren, S.; Qin, H.; Bu, J.; Zhu, G.; Xie, J.; Hu, J. Coexistence of electric field controlled ferromagnetism and resistive switching for TiO_2 film at room temperature. *Appl. Phys. Lett.* **2015**, *107*, 062404. [CrossRef]
66. Bu, J.; Liu, X.; Hao, Y.; Zhou, G.; Cheng, B.; Huang, W.; Xie, J.; Zhang, H.; Qin, H.; Hu, J. Electric field modulated ferromagnetism in ZnO films deposited at room temperature. *Appl. Phys. Lett.* **2018**, *112*, 162408. [CrossRef]
67. Chen, X.; Ma, X.; Yang, Y.; Chen, L.; Xiong, G.; Lian, G.; Yang, Y.; Yang, J. Comprehensive study of the resistance switching in $SrTiO_3$ and Nb-doped $SrTiO_3$. *Appl. Phys. Lett.* **2011**, *98*, 122102. [CrossRef]
68. Pan, F.; Gao, S.; Chen, C.; Song, C.; Zeng, F. Recent progress in resistive random access memories: Materials, switching mechanisms, and performance. *Mater. Sci. Eng. R Rep.* **2014**, *83*, 1–59. [CrossRef]
69. Li, Q.; Yan, S.S.; Xu, J.; Li, S.D.; Zhao, G.X.; Long, Y.Z.; Shen, T.T.; Zhang, K.; Zhang, J. Electrical control of exchange bias via oxygen migration across CoO-ZnO nanocomposite barrier. *Appl. Phys. Lett.* **2016**, *109*, 252406. [CrossRef]
70. Wang, Z.; Sun, Y.; Zhou, X.; Pan, F.; Song, C. Local control of exchange bias by resistive switching. *Phys. Status Solidi Rapid Res. Lett.* **2018**, *12*, 1800446. [CrossRef]
71. Wei, L.; Hu, Z.; Du, G.; Yuan, Y.; Wang, J.; Tu, H.; You, B.; Zhou, S.; Qu, J.; Liu, H.; et al. Full electric control of exchange bias at room temperature by resistive switching. *Adv. Mater.* **2018**, *30*, 1801885. [CrossRef]
72. Yuan, Y.; Qu, J.; Wei, L.; Zheng, R.; Lu, Y.; Liu, R.; Liu, T.; Chen, J.; Luo, L.; Du, G.; et al. Electric control of exchange bias at room temperature by resistive switching via Electrochemical Metallization. *ACS Appl. Mater. Inter.* **2022**, *14*, 26941–26948. [CrossRef]
73. Ji, H.; Wei, J.; Natelson, D. Modulation of the electrical properties of VO_2 nanobeams using an ionic liquid as a gating medium. *Nano Lett.* **2012**, *12*, 2988–2992. [CrossRef]
74. Lu, N.; Zhang, P.; Zhang, Q.; Qiao, R.; He, Q.; Li, H.B.; Wang, Y.; Guo, J.; Zhang, D.; Duan, Z.; et al. Electric-field control of tri-state phase transformation with a selective dual-ion switch. *Nature* **2017**, *546*, 124–128. [CrossRef] [PubMed]
75. Zehner, J.; Wolf, D.; Hasan, M.; Huang, M.; Bono, D.; Nielsch, K.; Leistner, K.; Beach, G. Magnetoionic control of perpendicular exchange bias. *Phys. Rev. Mater.* **2021**, *5*, L061401. [CrossRef]
76. Hasan, M.U.; Kossak, A.E.; Beach, G.S. Large exchange bias enhancement and control of ferromagnetic energy landscape by solid-state hydrogen gating. *Nat. Commun.* **2023**, *14*, 8510. [CrossRef] [PubMed]
77. Dasgupta, S.; Das, B.; Knapp, M.; Brand, R.A.; Ehrenberg, H.; Kruk, R.; Hahn, H. Intercalation-driven reversible control of magnetism in bulk ferromagnets. *Adv. Mater.* **2014**, *26*, 4639–4644. [CrossRef] [PubMed]
78. Singh, R.; Witte, R.; Mu, X.; Brezesinski, T.; Hahn, H.; Kruk, R.; Breitung, B. Reversible control of magnetism: On the conversion of hydrated FeF_3 with Li to Fe and LiF. *J. Mater. Chem. A* **2019**, *7*, 24005–24011. [CrossRef]
79. Wei, G.; Wei, L.; Wang, D.; Tian, Y.; Chen, Y.; Yan, S.; Mei, L.; Jiao, J. Reversible Control of the Magnetization of Fe_3O_4 via Lithium Ions. *Appl. Phys. Lett.* **2017**, *110*, 062404. [CrossRef]
80. Mustafa, Z.; Pravarthana, D.; Wang, B.; Yang, H.; Li, R.W. Manipulation of exchange bias effect via all-solid-state Li-ion redox capacitor with antiferromagnetic electrode. *Phys. Rev. Appl.* **2020**, *14*, 014062. [CrossRef]
81. Mustafa, Z.; Jabeen, N.; Hassan, N.U.; Jelani, M.; Muhammad, A.Q.; Sehar, F.; Nasir, N.; Idrees, A.; Hussain, A.; Bajaber, M.A. Realization of room temperature exchange bias effect in Co/NiO bilayer via all-solid-state Li-ion redox capacitor. *Ceram. Int.* **2023**, *49*, 2115–2120. [CrossRef]
82. Islam, M.A.; Zuba, M.; Debiase, V.; Noviasky, N.; Hawley, C.J. High capacity lithium ion batteries composed of cobalt oxide nanoparticle anodes and Raman spectroscopic analysis of nanoparticle strain dynamics in batteries. *Nanotechnology* **2018**, *29*, 075403. [CrossRef] [PubMed]
83. Zhang, F.; Li, Z.; Xia, Q.; Zhang, Q.; Ge, C.; Chen, Y.; Li, X.; Zhang, L.; Wang, K.; Li, H.; et al. Li-ionic control of magnetism through spin capacitance and conversion. *Matter* **2021**, *4*, 3605–3620. [CrossRef]

84. Li, H.; Hu, Z.; Xia, Q.; Zhang, H.; Li, Z.; Wang, H.; Li, X.; Zuo, F.; Zhang, F.; Wang, X.; et al. Operando magnetometry probing the charge storage mechanism of CoO lithium-ion batteries. *Adv. Mater.* **2021**, *33*, 2006629. [CrossRef] [PubMed]
85. Xiao, C.; Wang, H.; Usiskin, R.; van Aken, P.A.; Maier, J. Unification of insertion and supercapacitive storage concepts: Storage profiles in titania. *Science* **2024**, *386*, 407–413. [CrossRef] [PubMed]
86. Reddy, M.A.; Fichtner, M. Batteries based on fluoride shuttle. *J. Mater. Chem.* **2011**, *21*, 17059–17062. [CrossRef]
87. Rongeat, C.; Anji Reddy, M.; Witter, R.; Fichtner, M. Solid electrolytes for fluoride ion batteries: Ionic conductivity in polycrystalline tysonite-type fluorides. *ACS Appl. Mater. Inter.* **2014**, *6*, 2103–2110. [CrossRef] [PubMed]
88. Nowroozi, M.A.; Ivlev, S.; Rohrer, J.; Clemens, O. La_2CoO_4: A new intercalation based cathode material for fluoride ion batteries with improved cycling stability. *J. Mater. Chem. A* **2018**, *6*, 4658–4669. [CrossRef]
89. Nowroozi, M.A.; Clemens, O. Insights on the behavior of conversion-based anode materials for fluoride ion batteries by testing against an intercalation-based reference cathode. *ACS Appl. Energy Mater.* **2018**, *1*, 6626–6637. [CrossRef]
90. Sen, S.; Gupta, A.; Reddy, V.; Gupta, R. Study of training effect by Kerr microscopy measurement in Fe thin film implanted with F-ions. *Phys. B Condens. Matter* **2022**, *632*, 413733. [CrossRef]
91. De Rojas, J.; Salguero, J.I.N.; Ibrahim, F.; Chshiev, M.; Quintana, A.; Lopeandia, A.; Liedke, M.O.; Butterling, M.; Hirschmann, E.; Wagner, A.; et al. Magneto-ionics in single-layer transition metal nitrides. *ACS Appl. Mater. Inter.* **2021**, *13*, 30826–30834. [CrossRef]
92. Quarterman, P.; Hallsteinsen, I.; Dunz, M.; Meinert, M.; Arenholz, E.; Borchers, J.A.; Grutter, A.J. Effects of field annealing on MnN/CoFeB exchange bias systems. *Phys. Rev. Mater.* **2019**, *3*, 064413. [CrossRef]
93. Jensen, C.J.; Quintana, A.; Quarterman, P.; Grutter, A.J.; Balakrishnan, P.P.; Zhang, H.; Davydov, A.V.; Zhang, X.; Liu, K. Nitrogen-based magneto-ionic manipulation of exchange bias in CoFe/MnN heterostructures. *ACS Nano* **2023**, *17*, 6745–6753. [CrossRef] [PubMed]
94. López-Pintó, N.; Jensen, C.J.; Chen, Z.; Tan, Z.; Ma, Z.; Liedke, M.O.; Butterling, M.; Wagner, A.; Herrero-Martín, J.; Menéndez, E.; et al. Room-Temperature Solid-State Nitrogen-Based Magneto-Ionics in $Co_xMn_{1-x}N$ Films. *Adv. Funct. Mater.* **2024**, *34*, 2404487. [CrossRef]